

This article was downloaded by:

On: 15 January 2011

Access details: *Access Details: Free Access*

Publisher *Taylor & Francis*

Informa Ltd Registered in England and Wales Registered Number: 1072954 Registered office: Mortimer House, 37-41 Mortimer Street, London W1T 3JH, UK



Journal of Experimental Nanoscience

Publication details, including instructions for authors and subscription information:

<http://www.informaworld.com/smpp/title~content=t716100757>

Synthesis and functionalities of noble metal nanoparticles formed through simple all-inorganic photochemical procedures

David Riassetto^a; Francine Roussel^b; Laetitia Rapenne^a; Hervé Roussel^a; Stéphane Coindeau^b; Odette Chaix^a; Fabrice Micoud^c; Marian Chatenet^c; Michel Langlet^a

^a LMGP, Grenoble Institute of Technology-Minatec, Grenoble 38016, France ^b CMTC, Grenoble Institute of Technology, France ^c LEPMI, Grenoble Institute of Technology, France

First published on: 18 January 2010

To cite this Article Riassetto, David , Roussel, Francine , Rapenne, Laetitia , Roussel, Hervé , Coindeau, Stéphane , Chaix, Odette , Micoud, Fabrice , Chatenet, Marian and Langlet, Michel(2010) 'Synthesis and functionalities of noble metal nanoparticles formed through simple all-inorganic photochemical procedures', Journal of Experimental Nanoscience, 5: 3, 221 – 243, First published on: 18 January 2010 (iFirst)

To link to this Article: DOI: 10.1080/17458080903470725

URL: <http://dx.doi.org/10.1080/17458080903470725>

PLEASE SCROLL DOWN FOR ARTICLE

Full terms and conditions of use: <http://www.informaworld.com/terms-and-conditions-of-access.pdf>

This article may be used for research, teaching and private study purposes. Any substantial or systematic reproduction, re-distribution, re-selling, loan or sub-licensing, systematic supply or distribution in any form to anyone is expressly forbidden.

The publisher does not give any warranty express or implied or make any representation that the contents will be complete or accurate or up to date. The accuracy of any instructions, formulae and drug doses should be independently verified with primary sources. The publisher shall not be liable for any loss, actions, claims, proceedings, demand or costs or damages whatsoever or howsoever caused arising directly or indirectly in connection with or arising out of the use of this material.

Synthesis and functionalities of noble metal nanoparticles formed through simple all-inorganic photochemical procedures

David Riassetto^{a*}, Francine Roussel^b, Laetitia Rapenne^a, Hervé Roussel^a, Stéphane Coindeau^b, Odette Chaix^a, Fabrice Micoud^c, Marian Chatenet^c and Michel Langlet^a

^aLMGP, Grenoble Institute of Technology – Minatec, Grenoble 38016, France; ^bCMTC, Grenoble Institute of Technology, Saint Martin d'Hères 38402, France; ^cLEPMI, Grenoble Institute of Technology, Saint Martin d'Hères 38402, France

(Received 1 July 2009; final version received 7 November 2009)

The photochemical reduction of metal precursors under UV light has been studied to produce noble metal nanoparticles. Depending on the metal (Pt, Au or Ag) and precursor (chlorinated or nitrate) natures, different 1-step or 2-step photolytic or photocatalytic reduction mechanisms have been investigated. These mechanisms yield simple all-inorganic methods to generate metal nanoparticles in liquid medium and disperse these particles at the surface of various kinds of supports. Depending on the metal particle and support natures, different functionalities can arise from such easy and low-cost photometallisation methods.

Keywords: photochemistry; noble metals; nanoparticles; photolysis; photocatalysis

1. Introduction

Soft chemistry methods can advantageously be used to form metal nanoparticles in liquid suspensions. These methods often involve a reduction of metal precursors in liquid medium through photochemical mechanisms. They lead to colloidal suspensions of metal nanoparticles, which can, in turn, be dispersed on various substrates in atmospheric conditions. Such protocols yield low-cost procedures that cover a large field of applications, including (photo) catalysis, (photo) electrochemistry, optics, plasmonic or sensors [1–3]. These photochemical methods generally rely on rather complex chemical formulations involving organic or metal–organic additives used as reductive, capping and/or surfactant agents [4–8]. These additives play a key role in the fine control of the mean size, size distribution and stability of metal nanoparticles in liquid solutions. For instance, the use of NaBH₄ or citrate additives is very well documented in the literature [3,9–16]. Owing to the efficiency of these methods, little attention has been paid to the optimisation of all-inorganic photochemical (AIP) reductive protocols yielding

*Corresponding author. Email: David.Riassetto@grenoble-inp.fr

metal nanoparticles, i.e. protocols, which do not involve any organic or metal–organic additives.

However, when such additives remain fixed at the surface of metal nanoparticles, and they can reduce or thwart functionalities of these particles in various application fields. While antibacterial properties of noble metal nanoparticles, e.g. silver nanoparticles, are often studied for garment or medicinal applications [17–20], organic residues present at the metal surface can provoke biological hazards [21]. While noble metal nanoparticles, e.g. platinum nanoparticles, distributed at the surface of TiO₂ photocatalysts can enhance the photocatalytic activity [15,22–29], organic residues can alter or cancel this activity [2,30]. While metal platinum nanoparticles are the objects of tremendous interest for electrode applications in proton exchange membrane fuel cells (PEMFC) [2,31–35], the oxidation of organic residues present at the surface of these nanoparticles, yielding the formation of adsorbed carbon monoxide, can dramatically reduce the efficiency of such electrodes [2,30]. Finally, and from a general point of view, it is obvious that any technical simplification or cost reduction arising from the development of simplified AIP formulations can present practical interests for industrial applications.

Thus, the study and optimisation of AIP reductive protocols yielding metal nanoparticles, i.e. AIP metallisation protocols, remains of high interest both from academic and applicative points of view. In this context, we have studied several AIP routes. The aims of this article are twofold. We first present detailed studies which show, on the basis of previously published [36] and more recent observations, how AIP routes can yield the controlled formation of metal platinum nanoparticles of good size uniformity. In order to illustrate the potential of these AIP platinisation routes, some functionalities arising from the so-formed platinum nanoparticles are also presented. Then, we present first feasibility studies showing how protocols developed for platinum nanoparticles can be extrapolated or adapted to metal gold and silver nanoparticles. Differences in mechanisms involved in various AIP procedures are discussed in relation to the metal nature.

2. Experimental

2.1. Materials

In this study, sol–gel TiO₂ photocatalytic films have routinely been used as model dispersion supports for AIP-derived metal particles. TiO₂ films were deposited from two kinds of solutions. A mother solution (MS) was prepared from tetraisopropyl orthotitanate (TIPT) diluted in a solution containing ethanol, water and hydrochloric acid, with a TIPT concentration of 0.4 M, a pH of 1.27 and a water to TIPT molar ratio of 0.8. Crystalline suspensions (CS) of TiO₂ anatase nanoparticles were prepared from this MS. The preparation essentially relied on the autoclaving of a modified MS solution, which finally yielded a CS with a 0.24 M concentration of TiO₂ crystallites in ethanol. Both MS and CS protocols have been fully detailed in our previous papers [37,38]. TiO₂ films were then deposited at room temperature on (100) silicon wafers or soda-lime glasses (3.3 × 3.3 cm⁻²) by spin coating. The room temperature MS and CS deposition yielded a wet amorphous gel film and a wet crystalline film, respectively. MS-derived TiO₂ films were crystallised by heating at 500°C for 2 h. CS-derived TiO₂ films were only dried at 110°C for 2 h. Our previous studies showed that both the procedures yielded

well-crystallised TiO₂ films, which in turn governed their photocatalytic activities [37,38]. The MS and CS TiO₂ film thicknesses were fixed at 250 and 300 nm, respectively, using a multilayer deposition procedure. For comparison, commercial indium tin oxide (ITO) films on glass (purchased from Sigma-Aldrich) and TiO₂ powders (P25, from Degussa) were also punctually tested as alternative dispersion supports of metal nanoparticles.

2.2. Photometallisation conditions

Photometallisation experiments were performed using chloroplatinic acid hexahydrate (CPA, H₂PtCl₆ · 6H₂O), chloroauric acid hydrate (CAA, HAuCl₄ · H₂O) and silver nitrate (SN, AgNO₃), as platinum, gold and silver precursors, respectively. In all cases, these experiments were performed in a water/ethanol liquid medium of 80/20 M composition, according to our previous studies [39]. Photometallisation in liquid solution was achieved under UV exposure using three UVA lamps (PLS 11 W, from Philips). These lamps exhibit a continuous emission spectrum extending from 350 to 400 nm with an emission maximum centred at around 365 nm, i.e. they do not emit in the UVB/UVC spectral range. Solutions exposed to UV light were settled in a UV transparent container, whose bottom was fixed at 2 cm from the lamps. At this distance, UV light power at 365 nm was measured to be around 5 mW/cm⁻². When UV light experiments were performed in the presence of a TiO₂ thin film sample, the latter was positioned at a distance of 8 mm from the container bottom, the coated surface being oriented towards the lamps. Two generic AIP metallisation protocols were studied to form nanoparticles and disperse them at the surface of TiO₂ films or other supports.

2.2.1. 1-Step AIP method

A 1-step AIP protocol was implemented to load metal particles on TiO₂ films. A TiO₂-coated substrate was settled on a sample holder and immersed in the solution containing metal precursors. Sample and solution were then exposed to UV light in a climatic cabinet regulated at 20°C temperature and 40% relative humidity. Metallised films were then rinsed with deionised water and subsequently dried in air at 110°C for 2 h.

2.2.2. 2-Step AIP method

A 2-step method was also implemented. Solutions containing metal precursors were preliminarily exposed to UVA light in the absence of any TiO₂ film. A TiO₂- or ITO-coated substrate was then immersed in the preinsolated solution, using the same experimental device and conditions as the 1-step method, but without UV illumination. After immersion, the supports were rinsed with deionised water and subsequently dried in air at 110°C for 2 h. Some variations of this protocol could also be adapted to load metal particles on TiO₂ P25 pigments, which will be presented in the following sections.

As will be illustrated and discussed hereafter, both protocols yielded the formation of metal particles within the solution and/or at the solid surface. In both cases, the amount of metal particles distributed at the solid surface was controlled through variations in the film immersion duration within liquid solutions of various concentrations eventually preinsolated for various durations. Quantitative data concerning these parameters are provided in the following sections.

2.3. Characterisation methods

In order to study mechanisms occurring over UV exposure, UV-visible measurements were performed in transmission, on liquid solutions or films deposited on glass, using a Jasco V-530 spectrophotometer. UV-visible characterisations of solutions were performed on small aliquots periodically, withdrawn during UV exposure. Surface imaging of metallised films was performed using a ZEISS Ultra 55 field electron gun scanning electron microscope (FEG-SEM) operated at 20 kV. A Philips XL 30 scanning electron microscope operated at 6 kV was used for energy dispersive X-ray (EDX) analyses. TEM imaging was performed using a JEOL-2010 LaB6 instrument operated at 200 keV. X-ray diffraction (XRD) measurements were performed in $\theta/2\theta$ configuration, on platinum and gold particles collected from AIP-derived solutions, using a Siemens D500 diffractometer. XRD measurements were performed in grazing incidence, on TiO₂ films loaded with AIP-derived silver particles, using a PANalytical X'Pert Pro MPD diffractometer with a 0.29° incidence angle. Both apparatus used a Cu-K α X-ray source ($\lambda = 0.1541$ nm). Raman spectra were acquired with a Jobin-Yvon LabRam spectrophotometer, using an Argon laser source ($\lambda = 480$ nm) and a 25 s integration time. Photocatalytic properties of metallised TiO₂ films were studied through the oxidative photodecomposition of Orange G (5×10^{-5} M in aqueous solution), using the same device as that utilised for photometallisation experiments and according to a previously detailed protocol [39]. Voltammetric characterisations were also performed using a homemade 4-electrodes cell equipped with a rotating working electrode, according to a previously detailed protocol [33,40]. These characterisations were realised to assess the electro-reduction of gaseous oxygen in liquid solution, i.e. an aqueous solution of H₂SO₄ (0.1 M) saturated with gaseous oxygen in the presence of a vitreous carbon electrode coated with platinumised TiO₂ P25 pigments.

3. Results and discussions

3.1. AIP platinisation protocols

Mechanisms occurring during the 1-step or 2-step AIP platinisation of TiO₂ films have previously been studied through UV-visible spectrometry measurements in liquid solutions exposed to UV light [36]. We showed that the AIP platinisation was governed by a photolytic reduction mechanism occurring within the CPA precursor solution, rather than a photocatalytic reduction at the TiO₂ film surface. Chlorinated metal complexes in liquid solution, such as CPA or CAA, are absorbed in a wide UV spectral range that extends over the emission range of our UVA lamps. Thus, as will be illustrated in Section 3.4, in the case of CAA, these complexes undergo a multistep photolytic reduction when exposed to our UVA lamps, without the need of any reductive additive in the solution [41]. In the case of platinum complex, this mechanism initially involves a photo-induced homolytic cleavage of the Pt–Cl bond, inducing a first reduction of Pt⁴⁺ ions and the formation of Cl° (chlorine radical) radicals. These radicals can in turn react with an oxidisable reactant, such as ethanol present in our solution, yielding new radicals that participate in further reduction of platinum cations. Thus, though literature indicates that such a mechanism has not been fully exploited, we have shown in our previous work that, in suitable conditions, it is possible to form Pt° (metallic platinum) metal nanoparticles through a well-controlled process without the need of any reductive additive [36]. Loading of the so-formed platinum

particles on solid surfaces can be easily achieved either through a 1-step AIP procedure, which involves an *in-situ* surface platinisation during photolytic reduction of the CPA solution, or through a 2-step AIP procedure, which involves a prephotolysis step followed by a subsequent adsorption of platinum particles at the solid surface. X-ray photoelectron spectroscopy measurements demonstrated that both 1-step and 2-step methods yielded platinum particles with a similarly strong metallisation degree [36]. We also showed that 1-step and 2-step procedures yielded the surface dispersion of spherical particles with a bimodal size repartition, i.e. a 2- and 20-nm diameter for the smallest and biggest particles, respectively.

New studies have been performed to assess how the size of platinum particles distributed at the surface of TiO₂ films can be influenced by platinisation conditions. As illustrated by the FEG-SEM images of Figure 1, this size is primarily influenced by the UV exposure duration in relation to the concentration of CPA in solution. For a CPA solution of 860 μM concentration, Figure 1(a) shows that a 1-step procedure of short duration (1 h or less) essentially yields the dispersion of 20-nm particles (see white spots). Similar results were obtained when implementing a 2-step procedure with a prephotolysis step of comparable duration (Figure 1(b)). The TEM image shown in Figure 2(a) indicates that such particles consist of polycrystalline aggregates constituted of 2-nm primary particles, whose crystalline state is clearly evidenced by the observation of crystallographic planes (see circles). During the synthesis in liquid solution, very small clusters formed in the early stages of synthesis are prone to be re-diluted owing to their meta-stable state [42–44]. Above a certain critical size, stable particles can no longer be re-diluted. It seems that, in our conditions, the 2-nm diameter corresponds to this critical size. However, owing to their very small size, such particles present a high surface energy. In order to minimise this energy, i.e. the size of particles diluted in liquid solution, these particles tend to rapidly agglomerate. This agglomeration mechanism can partly explain the formation of 20 nm polycrystalline aggregates illustrated in Figures 1(a), (b) and 2(a). Agglomeration also depends on the contact probability of particles, which in turn relies on the particle concentration in liquid solution, i.e. a greater concentration favours a more efficient agglomeration. Accordingly, Figure 1(c) shows that, when a 1-step procedure is implemented using a very diluted CPA solution of 23 μM, i.e. when reducing the contact probability between particles in solution, only 2 nm particles are dispersed at the TiO₂ film surface after a short 1-step photoplatinisation of 1 h or less. These observations illustrate a way to selectively control the dispersion of very small and uniform platinum particles at the TiO₂ film surface using a simple 1-step AIP procedure. We previously showed that the amount of the so-formed particles distributed at the film surface could be flexibly monitored through the film immersion duration under UV light [36].

Figure 1(d) shows that, when using a 1-step procedure with a CPA solution of 860 μM concentration, the amount of 20-nm particles diminishes when increasing the UV irradiation duration. At the same time, 2 nm particles appear at the film surface. Actually, prolonged immersion durations, for around 15 h, yielded films exclusively, but rather heterogeneously, coated with 2-nm particles [36] (not illustrated here). In contrast, when implementing a 2-step procedure, Figure 1(e) shows that it is possible to selectively disperse 2 nm particles at the film surface after a prolonged prephotolysis step of around 15 h. This figure also illustrates the good size homogeneity of the so-formed particles and their uniform distribution at the film surface. The TEM image presented in Figure 2(b)

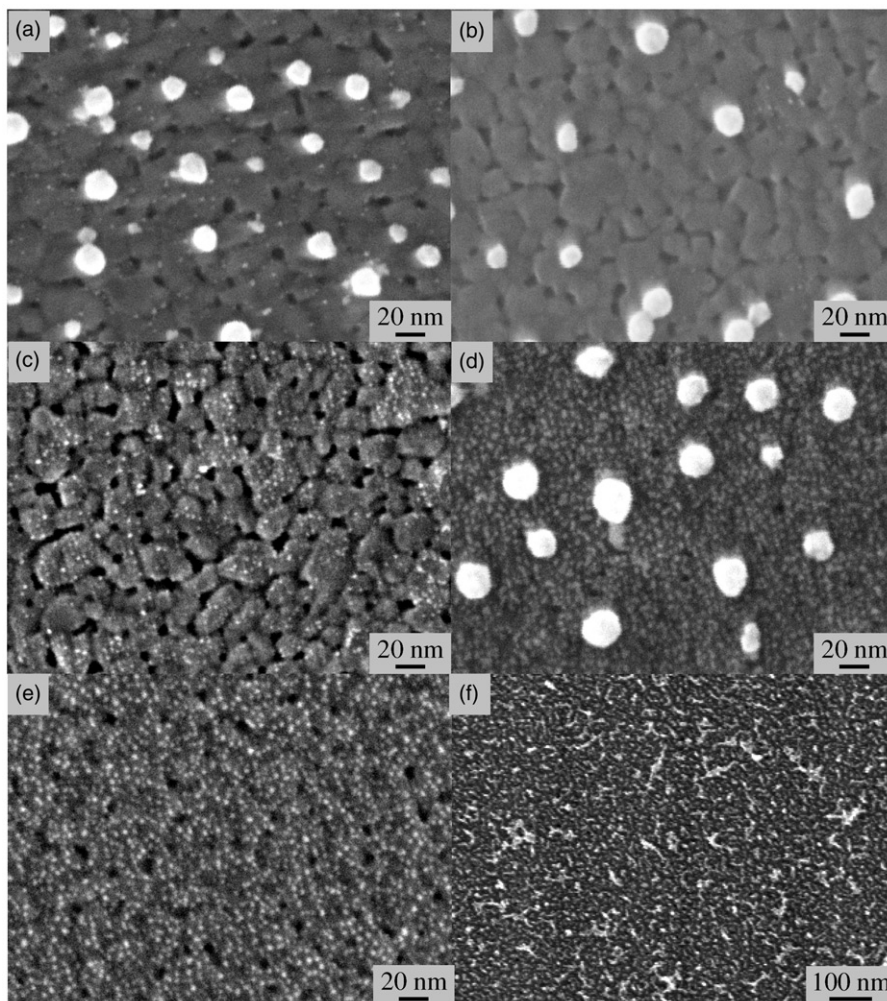


Figure 1. FEG-SEM surface images of 250 nm thick MS TiO_2 films platinised through AIP procedures. A 1-step platinisation procedure was implemented with a film immersion for 30 min in an 860 μM (a) or a 23 μM CPA solution (c) and a film immersion for 4 h in an 860 μM CPA solution (d). A 2-step platinisation procedure was implemented, which involved a film immersion for 5 min in an 860 μM CPA solution prephotolysed for 45 min (b) or 15 h, before (e) or after ageing this solution for several weeks (f).

confirms the 2 nm diameter of these particles and their single-crystal state is depicted by clearly observable crystallographic planes (see circles). This crystalline state has also been confirmed by XRD on a powder collected after a 15 h photolysis. The XRD pattern illustrated in Figure 3(a) indicates a pure phase crystallised in the face-centred cubic structure of metallic platinum (ICDD card # 01-071-3756). The mean diameter of 3–4 nm, deduced from this XRD pattern using the Debye–Scherrer relationship, is in rather good agreement with the 2 nm value estimated from FEG-SEM (Figure 1(e)) and TEM images (Figure 2(b)). All these observations illustrate a new way to selectively control the

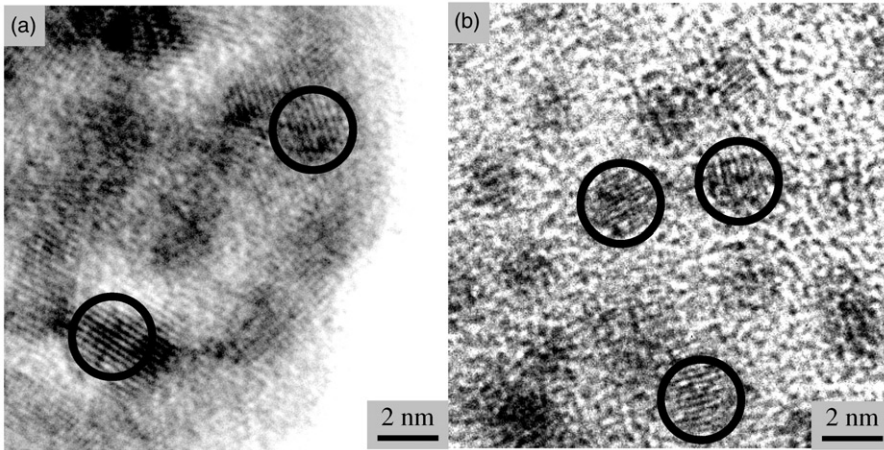


Figure 2. TEM images of platinum particles derived from an 860 μM CPA solution prephotolysed for 45 min (a) and 15 h (b). Circles indicate individual platinum particles.

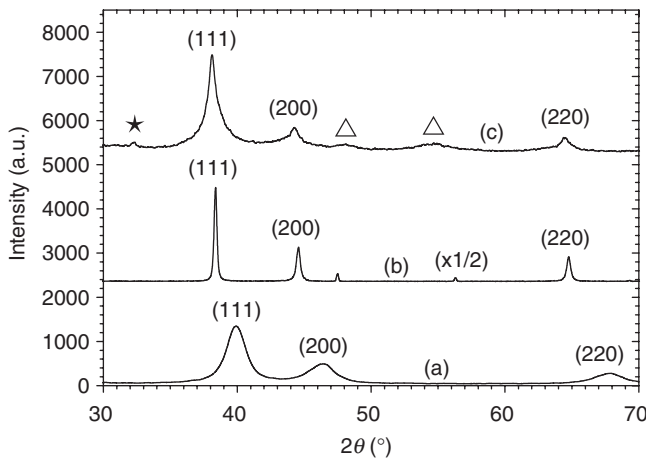


Figure 3. XRD patterns for metal powders collected from a CPA solution photolysed for 15 h (a) and a CAA solution photolysed for 3 h (b) and for silver particles loaded on a TiO_2 MS film immersed for 5 min within a 100 mM SN solution using a 1-step AIP protocol (c). Reflections of the Pt° (metallic platinum), Au° (gold) and Ag° (silver) face-centred cubic structures are indexed. Additional symbols in (c) depict the TiO_2 support (triangles) and indicate the existence of a minor secondary Ag_2O component (star).

dispersion of well-calibrated and very small particles at the TiO_2 film surface using a simple 2-step AIP procedure. In our previous article, we showed that, in these conditions, the amount of loaded platinum particles could be precisely monitored through a suitable adjustment of the platinum concentration and/or immersion duration of the film in the prephotolysed solutions [36].

3.2. Photo-induced mechanisms

Besides photolytic reduction mechanisms yielding the formation of noble metal nanoparticles in liquid solution, several authors have reported that the so-formed particles can undergo various structural and morphological changes when exposed to UV or visible light. These effects are related to the excellent photochemical activity of such nanoparticles, which in turn relies on their high-surface/volume ratio and unusual electronic properties. Two different effects have been reported, which can not only take place under high-intensity light excitation but also under rather low-intensity excitation, such as in our experimental conditions [15,45–49]. On the one hand, single nanoparticles or aggregates of nanoparticles can undergo a photofragmentation when subjected to UV irradiation in liquid solution [15,46,49]. This mechanism would arise from a photo-induced generation of electrons within metal nanoparticles or nanoaggregates. These electrons are prone to be ejected towards the surrounding liquid, yielding positively charged metal particles [15,46,49]. However, before ejection, photoelectrons can induce a first destabilisation of metal nanoparticles or nanoaggregates, followed by their subsequent fragmentation yielding the formation of smaller metal clusters. On the other hand, when nanoparticles exist in the form of aggregates, it has been reported that UV or visible light excitation can cause their photofusion [15,45,48]. Such a mechanism would arise from a photo-induced increase of the nanoparticle temperature, which would promote a partial melting followed by the coalescence of vicinal particles yielding the formation of larger single particles. The occurrence of a photo-induced fragmentation or fusion depends on many factors, such as the nature and morphology of metal particles, as well as the light exposure conditions. According to the aforementioned mechanisms, it is believed that the disappearance of 20 nm platinum particles and the appearance of 2 nm ones over UV exposure, as illustrated in Figure 1, depict a photo-induced fragmentation of initially formed polycrystalline aggregates. This fragmentation would take place either at the film surface (Figure 1(a) and (d)) or in the solution (Figure 1(b) and (e)). Such a photofragmentation has extensively been described for gold and silver nanoparticles [15,46,49] but, as far as we know, has never been reported in the case of platinum nanoparticles. Thus, a more precise assessment of this mechanism will require further studies.

Some studies have been performed to assess the stability over a time of 860 μM CPA solution photolysed for 15 h. We observed that the morphology of platinum particles, distributed at the surface of a TiO_2 film using a 2-step AIP procedure, remained unchanged after ageing such a solution in ambient conditions for some hours, i.e. remained similar to that depicted in Figure 1(e) (not illustrated here). This observation reinforces the potential of a 2-step AIP platinisation route, which does not involve any stabilising additive, such as surfactant or else, in the solution. However, UV-visible spectrometry measurements performed on this solution show that further ageing in ambient conditions yields slow modifications. It is illustrated in the spectra of Figure 4(a) and (b) for a non-aged solution or a solution aged for 36 h, respectively. As detailed in our previous article, such spectrum evolutions depict structural or morphological changes of the platinum particles in solution [36]. Figure 1(f) shows a FEG-SEM image of platinum particles distributed at the surface of a TiO_2 film using a 2-step procedure, with such a solution aged for a prolonged period of several weeks. Compared to Figure 1(e), Figure 1(f) depicts a significant growth as well as a strong broadening in the size and shape distribution of particles distributed at the film surface. Thus, data of Figures 1(e) and (f)

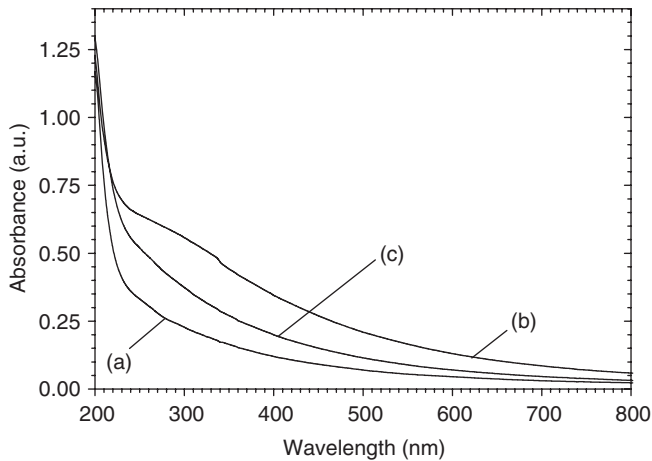


Figure 4. UV-visible spectra of an 860 μM CPA solution exposed to UV light for 15 h before (a) and after ageing in ambient conditions for 36 h (b) and exposed to UV light for 4 days (c).

and 4(a) and (b) illustrate certain instability of the solution photolysed for 15 h. Conversely, a comparison between the spectra of Figure 4(a) and (c) shows that solution evolutions are considerably reduced when this solution is aged under UV light. It is believed that such a solution stabilisation promoted by UV light arises from the aforementioned photo-induced generation of (probably positively) charged metal particles, which would reduce their interactions through electrostatic repulsion mechanisms in liquid solution. This observation has two major consequences. It reinforces the assumption of photo-induced charge effects, which may eventually promote a photofragmentation of platinum particles in solution, and it indicates an easy way to stabilise platinum particles in liquid solution before their dispersion on a solid surface through a 2-step AIP route, without using any stabilising additive in the solution.

3.3. Functionalities of AIP-derived platinum nanoparticles

As illustrated earlier, a 1-step AIP procedure yields an easy *in-situ* platinisation of TiO_2 photocatalytic films. The photocatalytic activity of TiO_2 films concerns, for instance, applications for self-cleaning surfaces or devices for water purification or air decontamination [23]. Figure 5 illustrates the beneficial effects of platinum particles dispersed at the TiO_2 film surface using a 1-step AIP procedure of short duration (30–60 min). It is observed that platinisation yields a considerable enhancement of the film photoactivity, by a factor around 4 compared to a non-platinised film. This improvement is due to well-known Schottky barrier effects taking place at Pt/ TiO_2 interfaces, which favour a more efficient separation of charge carriers photogenerated in the TiO_2 semiconductor under UV light [39]. This charge carrier separation promotes, in turn, a more efficient oxidative photodecomposition of molecules adsorbed at the film surface. Such a mechanism has extensively been described for powder photocatalysts, but is very rarely exploited for thin film photocatalysts. Thus, data illustrated in Figure 5 illustrates the interest of our AIP

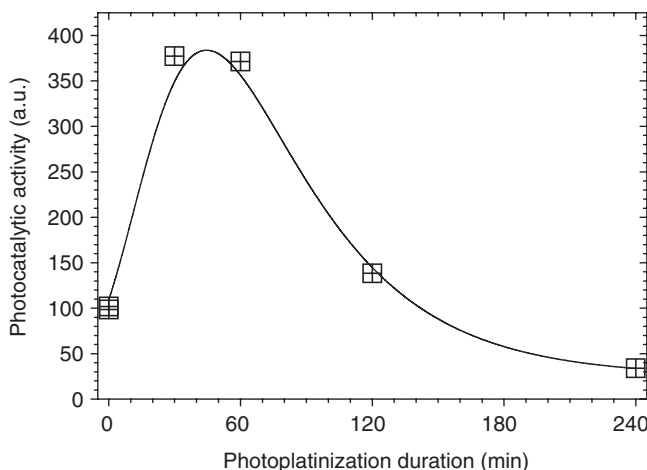


Figure 5. Influence of the 1-step AIP platinisation duration on the photocatalytic activity of 250 nm thick platinised MS TiO₂ films. The films were platinised using a 860 μM CPA solution.

procedure for photocatalytic applications. However, this figure also shows that a prolonged 1-step platinisation procedure induces a drop in the photocatalytic activity of platinised films. This feature suggests that there exists an optimal platinum loading threshold above which platinum particles may alter the film photoactivity. Besides, since smaller size platinum particles are produced when increasing the 1-step platinisation duration (Figure 1(a) and (d)), size effects can also influence photocatalytic activity decreases. These features are out of the topics of this work and have been the object of extensive studies published in a recent article [50].

As shown earlier, a 2-step AIP procedure with a prolonged prephotolysis step yields the homogeneous distribution of well-calibrated small platinum particles at the surface of TiO₂ films. This procedure is obviously not restrained to TiO₂ films and many other kinds of supports can easily be platinised using such a procedure. This aspect is first illustrated in Figure 6(a), which shows a FEG-SEM image of an ITO-on-glass sample immersed within a CPA solution prephotolysed for 15 h. This figure clearly evidences the presence of 2-nm platinum particles homogeneously dispersed on the ITO film. Platinum dispersion at an ITO surface can present interests for electrochemical applications such as new electrode materials [51], and these aspects will be the object of future studies. The 2-step AIP protocol is not either restrained to thin film supports. It is illustrated in the TEM image of Figure 6(b), which shows platinised P25 TiO₂ pigments. For this experiment, 0.05 g of TiO₂ were immersed for 10 h in 200 cc of a 860 μM CPA solution prephotolysed for 15 h. The resulting powder was filtered, then rinsed with deionised water and subsequently dried in air at 110°C for 2 h. The TEM image of Figure 6(b) clearly shows 2 nm platinum particles (see dark spots) uniformly distributed at the surface of TiO₂ pigments. For these platinisation conditions, inductively coupled plasma absorption emission spectroscopy measurements revealed a Pt/TiO₂ ratio of 22 weight%, which illustrated the high efficiency of our AIP platinisation procedure.

Platinised TiO₂ pigments are the objects of much interest as alternative cathodes in PEMFC applications for the electroreduction of gaseous oxygen [2,31–35]. In order to

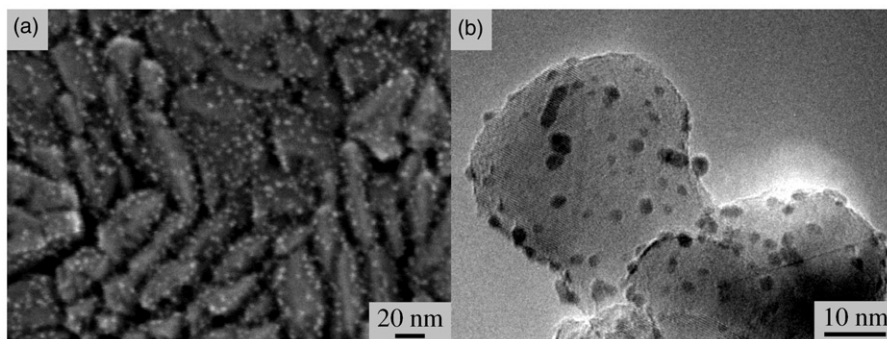


Figure 6. FEG-SEM surface image of a platinised ITO-on-glass sample (a) and TEM image of platinised P25 TiO_2 pigments (b). Platinisation was performed using a 2-step AIP method with an $860 \mu\text{M}$ CPA solution photolytised for 15 h.

assess the potential of our AIP method for such applications, platinised TiO_2 pigments have been deposited on a vitreous carbon electrode and voltammetric measurements have been performed. For comparison, these measurements have also been performed on a commercially available electrocatalyst (Pt/C, E-TEK) constituted of platinised carbon powders with a platinum loading, comparable to our platinised TiO_2 pigments. Figure 7 shows voltamperograms measured on both kinds of samples for various rotation speeds of the working electrode. The measured current density becomes negative below a certain voltage threshold and tends to saturate at a low voltage. These trends illustrate the electroreduction of oxygen [52]. The maximal current density modulus, i.e. the saturation value, is also observed to increase when increasing the electrode rotation speed, which indicates that the reduction kinetics increases when increasing the flux of matter [52]. A comparison between our sample and the commercial reference indicates that, for all electrode rotation speeds, electroreduction of oxygen starts below a voltage value of around 0.9 V (versus RHE), which is only 0.1 V weaker than the threshold value measured for the reference, and the current density modulus is only 10% weaker than that measured for the reference. Thus, these first trials give promising results and it is hoped that further optimisations can yield performing PEMFC cathodes derived from our AIP protocol.

3.4. Extrapolation to gold nanoparticles through a 2-step AIP procedure

Since chlorinated metal complexes in liquid solution, such as CPA- or CAA-derived ones, are absorbed in the emission range of our UVA lamps, we have studied how AIP photolytic mechanisms involved in the formation of platinum particles can be extrapolated to gold nanoparticles. Such particles dispersed at a solid surface can, for instance, be used as seeds for nanowire growth [53] or in plasmonic applications [54,55]. Similar to our previous studies performed on platinum particles [53], photo-induced mechanisms occurring in a CAA solution have been investigated by UV-visible spectrometry. Figure 8 illustrates the evolutions of a pure CAA precursor solution of $250 \mu\text{M}$ concentration exposed to UV light, i.e. a CAA solution exposed to UV light without the presence of any photocatalyst or reductive additive. Assignments of bands observed in these spectra are

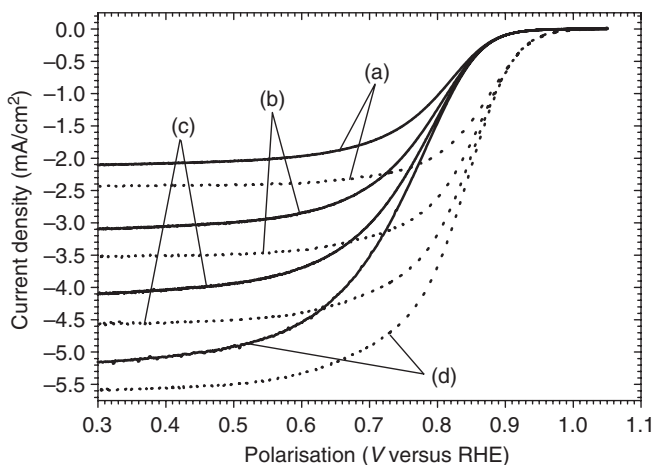


Figure 7. Voltamperograms, measured on platinised TiO_2 pigments (full lines) and a commercial reference (dotted lines) of comparable platinum loading, for an electrode rotation speed of 400 (a), 900 (b), 1600 (c) and 2500 rpm (d). Platinisation of TiO_2 pigments was performed using a 2-step AIP method with an $860\ \mu\text{M}$ CPA solution prephotolysed for 15 h.

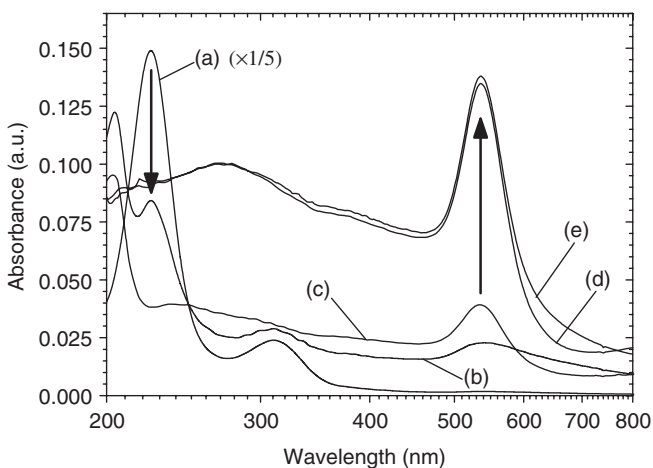


Figure 8. UV-visible spectra of a $250\text{-}\mu\text{M}$ CAA solution exposed to UV light for 0 (a), 2.5 (b), 45 (c) and 180 min, before (d) and after ageing in ambient conditions for two weeks (e).

summarised in Table 1. For the initial solution, a very intense band observed at 225 nm, and a weaker one at 310 nm, correspond to metal-to-ligand charge transfers in a chloraurate complex (Figure 8(a)) [56]. The CAA complex bands rapidly vanish over the very first minutes of UV exposure, which suggests a rapid photolytic reduction of the initial complex (Figure 8(b)). At the same time, a new band appears to grow at 205 nm. It has been reported that the photolytic generation of metal gold particles proceeds through a preliminary reduction of initial Au^{3+} cations into Au^+ ones, followed by a complementary reduction of these latter cations yielding Au^0 metal particles [57,58].

Table 1. Assignment of UV-visible bands illustrated in Figure 8.

Wavelength	205 nm	225 nm	270 nm	310 nm	535 nm
Assignment	Au ⁺ complex	CAA metal-to-ligand charge transfers	Metallic gold electronic transition	CAA metal-to-ligand charge transfers	Metallic gold plasmon band

We previously evidenced such a multistep reduction mechanism during the photolytic formation of platinum particles from CPA solutions [36]. It is therefore inferred that the 205 nm band observed in Figure 8(b) corresponds to partially reduced gold species.

Further increase of the UV exposure duration yields a progressive disappearance of the 205 nm band and the concomitant appearance of a new band located at 535 nm (Figure 8(c)). This latter band arises from plasmon resonance effects induced by metal gold nanoparticles [59]. After a prolonged UV exposure of 3 h, the total disappearance of initial Au³⁺ and Au⁺ bands is accompanied by an intensification of the plasmon band (Figure 8(d)), which means that photometallisation continuously proceeds over this period of UV exposure. Besides, a new band of weaker intensity appears at 270 nm. This latter band, which corresponds to an intrinsic electronic transition of metal gold particles [60,61], may eventually be already present in the spectrum of Figure 8(c) but would not be detected owing to its very weak intensity. In conditions illustrated in Figure 8, any evolution of the spectra could not be evidenced after a 3-h UV exposure (not illustrated here). It suggests that, after 3 h, gold metallisation has been completed. Data illustrated in Figure 8 shows, therefore, that the CAA complex exposed to UV light follows evolutions globally similar to those previously depicted from UV-visible characterisations performed on CPA solutions [36], i.e. a multistep photolytic reduction yielding metallic particles.

As for AIP-derived platinum particles, gold particles formed in the solution can be easily dispersed on solid supports through a simple 2-step AIP procedure. It is illustrated in the FEG-SEM image of Figure 9 for a TiO₂ film immersed for 1 h in a CAA solution prephotolysed for 3 h. Compared to platinum particles illustrated in Figure 1, this image depicts the surface distribution of rather larger particles of about 50 nm mean diameter. The metallic nature of these particles has been confirmed by XRD on a powder collected after a 3 h photolysis of the CAA solution. The XRD pattern of Figure 3(b) indicates a pure phase crystallised in the face-centred cubic structure of metallic gold (ICDD card # 00-004-0784). Besides, an average particle size of about 50 nm has been deduced from this XRD pattern using the Debye–Scherrer relationship, which confirms the particle size depicted in Figure 9. This observation indicates that, in contrast to platinum particles which initially consist of 20-nm aggregates prone to undergo photofragmentation over prolonged UV exposure, gold particles formed during the photolytic reduction of CAA actually consist of large single particles.

As aforementioned, owing to the strong photochemical activity of noble metal nanoparticles, photo-induced fragmentation or fusion mechanisms can be induced through the light exposition of metal particles in liquid solution. Such photo-induced mechanisms can strongly differ depending on the metal nature, which may in turn explain structural and morphological differences observed in this work for AIP-derived platinum

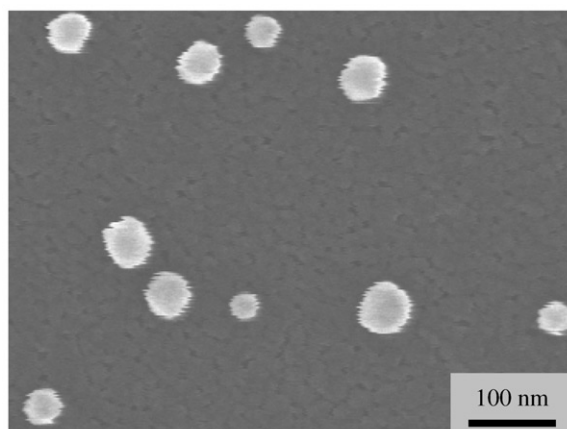


Figure 9. FEG-SEM image of gold nanoparticles loaded on a 250 nm thick MS TiO₂ film using a 2-step AIP procedure with a 3 h prephotolysis of a 250 μM CAA solution followed by a film immersion of 1 h.

and gold nanoparticles. It is possible that, in our AIP conditions and in contrast to platinum particles, gold particles undergo a photofusion mechanism in liquid solution rather than a photofragmentation one. A more precise assessment of these features will require further studies. However, the assumption of a photofusion of gold particles has two practical consequences. Since it would promote a growth of particles for a given concentration of particles in solution, the number of particles is supposed to progressively diminish, thus decreasing the interparticle contact probability. The growth kinetics is, therefore, expected to slow down over UV exposure. Moreover, since the photochemical activity of metal nanoparticles is supposed to promote a photo-induced charge generation and a subsequent formation of charged metal particles [15,45–49], it is inferred that these particles undergo repulsive electrostatic forces in liquid solution. Thus, a reduced contact probability associated to repulsive forces between charged particles can definitively stop the particle growth after a sufficient UV exposure duration. Accordingly, we have mentioned that, in conditions illustrated in Figure 8, no UV-visible spectrum evolution could be observed after a 3 h UV exposure. Such effects can also impact the stability of metal suspensions over ageing in ambient conditions. Accordingly, any decantation could not be observed after ageing for 2 weeks a gold solution photolysed for 3 h and very comparable spectra given in Figure 8(d) and (e) illustrates such stability. All these observations support the potential of an AIP procedure yielding gold particles without using any reductive or stabilising additive. Finally, the assumption of a photo-induced growth process suggests that the size of gold particles may be controlled through an adjustment of the UV exposure duration in relation to other parameters such as the CAA concentration in solution, which will be the object of further studies.

3.5. Adaptation to silver nanoparticles through a 1-step AIP procedure

Owing to its solubility in ethanol or water solution, we have chosen SN as a chemical precursor to study the AIP formation of silver particles. Contrary to platinum and gold

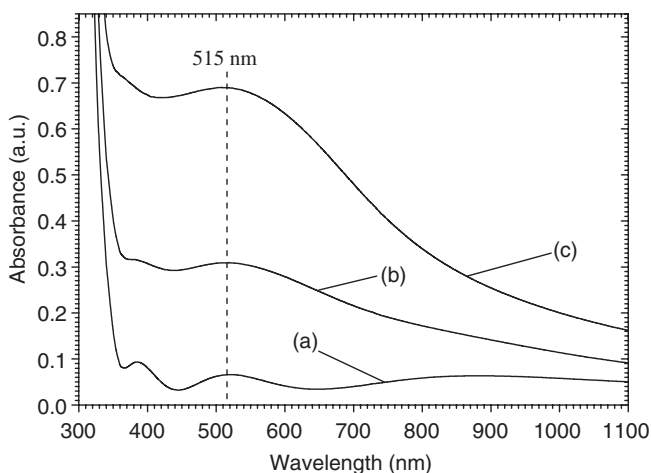


Figure 10. UV-visible absorbance spectra of a 300 nm thick TiO_2 CS film on glass before immersion (a) and after immersion for 5 min under UV light within a 1 (b) and a 100 mM SN solution.

chlorinated precursors, SN does not absorb in the emission range of our UVA lamps. Thus, no photolytic reduction can be expected from this precursor. In order to propose an alternative AIP reduction protocol, we have taken advantage of the TiO_2 photocatalytic properties. Let us recall that these properties involve the photogeneration of electrons and holes in titanium oxide exposed to UV light. In the presence of a sacrificial hole scavenger, ethanol in this work, photoelectrons and photoholes can be efficiently separated at a TiO_2 surface immersed in liquid medium and exposed to UV light. Photoholes are consumed by ethanol contacting the surface and photoelectrons can induce the reduction of species adsorbed at the surface [62]. This principle has been adapted to the photoreduction of SN through a 1-step AIP procedure. In other words, TiO_2 films have been immersed within water/ethanol SN solutions, and we have studied the photocatalytic reduction of Ag^+ cations adsorbed at the film surface exposed to UV light. Furthermore, we have tested this process on CS TiO_2 films. The CS protocol, as well as the post-metallisation one, only involves a heat treatment at 110°C . Thus, the whole procedure is compatible with many kinds of supports, including thermally sensitive substrates, which reinforces the potential interest of our AIP procedure.

Photoreduction features occurring at the TiO_2 film surface are illustrated by UV-visible spectra of Figure 10 for films deposited on glass and immersed for 5 min under UV light in SN solutions of various concentrations. Compared to the spectrum of a bare film (Figure 10(a)), spectra of Figure 10(b) and (c) depict a large band centred at around 515 nm and extending over a wide spectral range. Location and shape of this band closely corresponds to the plasmon band of metal silver nanoparticles dispersed at a solid surface [55,63–67]. Figure 10(b) and (c) also shows that, for the same immersion durations, the plasmon band intensity increases when increasing the SN concentration in solution. Thus, these spectra indicate that the photocatalytic metallisation of SN rapidly proceeds over a short UV exposure of 5 min and increasing the SN concentration in the solutions promotes faster metallisation kinetics. These features are confirmed by data of Figure 11,

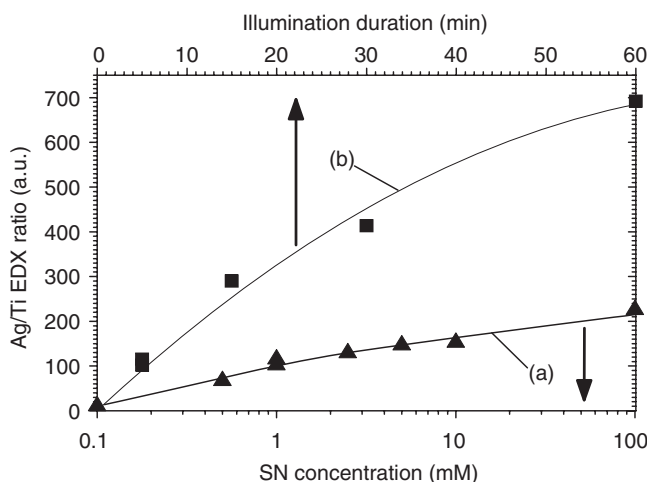


Figure 11. Variations of the Ag ($L\alpha$)/Ti ($K\alpha$) peak intensity ratio deduced from EDX analyses for 300 nm thick CS TiO_2 films loaded with silver particles using a 1-step AIP protocol. The film was immersed for 5 min in SN solutions of various concentrations (a) or for various durations in a 1 mM SN solution (b).

which illustrates variations of the Ag ($L\alpha$)/Ti ($K\alpha$) peak intensity ratio, as deduced from EDX analyses. It is observed that increasing the UV exposure duration or the SN concentration in solution promotes a gradual increase in the amount of loaded silver. Thus, data of Figures 10 and 11 shows that the photocatalytic reduction of SN provides an easy way to load metal silver particles at the surface of a TiO_2 film through a simplified 1-step AIP procedure.

Figure 12 illustrates FEG-SEM images of TiO_2 films loaded with silver particles. Figure 12(a) shows that a short film immersion of 5 min within a 1 mM SN solution exposed to UV light yields the uniform distribution of very small silver particles with a diameter of 5 nm or less (see bright spots highlighted by circles). Contrary to the images of Figure 1, for which the strong weight contrast between the TiO_2 support and platinum particles allows a clear visualisation of these particles, very small silver particles are only weakly visible in Figure 12(a) owing to a weaker weight contrast with the TiO_2 support. However, the TEM image shown in the inset of this figure confirms the very small size of these particles, and crystallographic planes observed in this image indicate their crystalline state. Figure 12(b) shows that increasing the immersion duration in a 1 mM solution yields a growth of silver nanoparticles and a broadening of their size distribution, which indicates a rather heterogeneous growth mechanism. In agreement with data of Figures 10 and 11, Figure 12(c) shows that the growth kinetics is accelerated when immersion is performed in a more concentrated SN solution of 100 mM. Figure 3(c) depicts the XRD pattern of silver particles loaded on a TiO_2 film in conditions illustrated in Figure 12(c). These particles essentially exhibit XRD reflections related to the face-centred cubic structure of metallic silver (ICDD card # 04-001-2617), which supports their metallic state. A very weak secondary reflection observed in this pattern can be assigned to a minor Ag_2O component, which probably depicts a partial surface oxidation of metal silver particles [68]. Other very

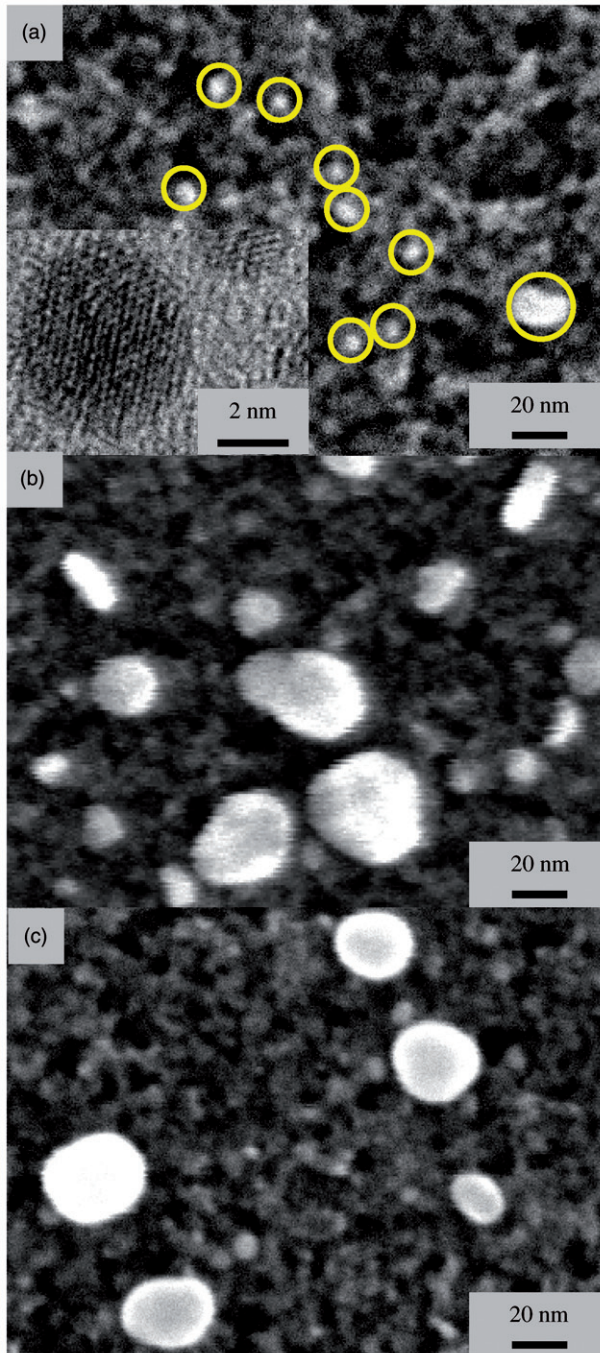


Figure 12. FEG-SEM images of 300-nm thick CS TiO_2 films loaded with silver nanoparticles using a 1-step AIP protocol. The film was immersed within a 1-mM SN solution for 5 (a) and 15 min (b), and for 5 min within a 100 mM SN solution (c). In (a), circles indicate the presence of very small silver particles, which are also illustrated by a TEM image in the insert of this figure.

minor reflections correspond to the TiO_2 support, which is weakly probed in a grazing incidence configuration used in this case. Besides, an average particle size of about 20 nm has been deduced from this XRD pattern using the Debye–Scherrer relationship. This size is in rather close agreement with the mean particle size depicted in Figure 12(c), which indicates that the growth mechanism illustrated in Figure 12(a) and (c) yields larger (non-agglomerated) single particles.

Thus, as for gold particles in liquid solution and in contrast to platinum ones, it seems that the photocatalytic reduction of SN at the surface of a TiO_2 film is governed by a photofusion mechanism of silver particles rather than a photofragmentation one. Such a photofusion mechanism occurring at the surface of an illuminated TiO_2 photocatalyst has already been reported for metal gold particles [48]. As illustrated in Figure 12(a), in early stages of metallisation, very small silver particles are sufficiently distant at the film surface to prevent such a growth mechanism. However, while new SN species are adsorbed and photocatalytically metallised particles are formed at the film surface, the interparticle contact probability increases and vicinal silver particles can undergo a photofusion process (Figure 12(b)). This process logically occurs all the more rapidly as SN solutions are more concentrated (Figure 12(c)). As illustrated in Figure 12(b) and (c), this growth mechanism does not totally proceed homogeneously, and it yields some broadening in the size distribution of silver particles distributed at the film surface. We have shown that the photocatalytic activity of CS TiO_2 films can be flexibly monitored through variations in the film thickness [37,38]. Thus, in future studies, it will be interesting to test how variations in the film photoactivity, in relation to other experimental parameters, can eventually reduce the size distribution of AIP-derived silver particles.

As illustrated in Figure 10, TiO_2 films loaded with silver particles exhibit a significant plasmon resonance. Surface plasmon effects cover many application fields [55]. They are, for instance, considered for photovoltaics devices, since surface plasmons significantly improve the absorption of light in such devices or for sub-wavelength optics applications. They are also involved, in association with specific chemical interactions, in surface enhanced Raman scattering (SERS) effects, which result in the strong exacerbation of the Raman signal arising from molecules attached to metal nanoparticles [3,13,48,69,70]. For instance, SERS effects are considered for sensor applications [3]. Figure 13 depicts the Raman spectrum of a 300 nm thick TiO_2 CS film before and after loading with silver nanoparticles using a 1-step AIP protocol with a film immersion for 1 h in a 1 mM SN solution. This figure shows that the presence of silver particles enhances the Raman detection of the supporting TiO_2 film by a factor 25 compared to a bare film, which demonstrates the SERS effect induced by AIP-derived silver particles. Of course, this enhancement is weak compared to what is commonly reported in the literature. However, it is worthwhile to note that spectra illustrated in Figure 13 cannot allow any quantification of the SERS activity. Indeed, the bare film spectrum accounts for the whole film thickness, while the exacerbated Raman signal arising from SERS effects only accounts for the extreme film surface in contact with silver particles. Finally, it should be mentioned that, while the photocatalytic formation of silver nanoparticles requires the presence a TiO_2 photocatalyst, this procedure is not necessarily restrained to a TiO_2 film surface functionalisation. Accordingly, we have also developed AIP protocols based on the photocatalytic reduction of SN diluted in a CS liquid suspension. These AIP protocols, which will be detailed in a future article, yield the formation of metal silver

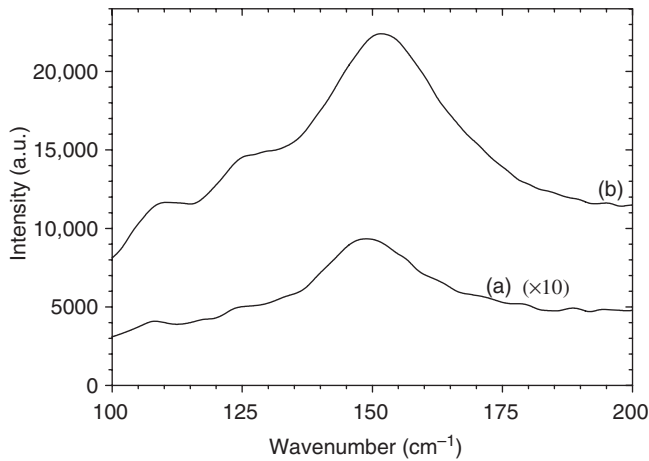


Figure 13. Main anatase Raman mode of a 300 nm thick CS TiO₂ film before (a) and after immersion for 1 h within a 1 mM SN solution using a 1-step AIP protocol (b). Both spectra have been collected with a same integration time of 25 s.

nanoparticles in liquid suspension, which can then be dispersed on various supports. These suspensions are presently under investigation in our group for antibacterial applications on textile supports, which in turn rely on the known antibacterial activity of silver nanoparticles [18].

4. Conclusion

Simplified and low-cost AIP methods, based on photolytic or photocatalytic mechanisms, have been studied to form metal platinum, gold or silver nanoparticles in liquid suspensions, without the need of any organic or metal–organic additive in the solution and to disperse these particles at the surface of various supports. These methods allow a flexible control in the amount of nanoparticles loaded at the support surface, through an adjustment of the support immersion duration in the solution and/or metal precursor concentration in the solution. A 1-step AIP procedure yields an easy *in-situ* way to load platinum particles at the surface of solid supports, while a 2-step AIP procedure allows the selective dispersion of 2 or 20 nm platinum particles. An extrapolation of this 2-step AIP procedure yields uniform gold particles of larger size, while an adaptation of the 1-step AIP procedure yields silver particles whose dimensions depend on the experimental conditions. It seems that the size of metal particles relies on photofragmentation or photofusion mechanisms, in relation to the metal particle natures and metallisation conditions. Different functionalities of AIP-derived metal particles show that these simplified and low-cost AIP methods present an interesting potential for different application fields. Further studies are necessary to better understand the photochemical mechanisms involved in the formation of metal nanoparticles and how these mechanisms influence the size and morphology of these particles.

References

- [1] M.C. Daniel and D. Astruc, *Gold nanoparticles: Assembly, supramolecular chemistry, quantum-size-related properties, and applications toward biology, catalysis, and nanotechnology*, Chem. Rev. 104 (2004), pp. 293–346.
- [2] K.-Y. Chan, J. Ding, J. Ren, S. Cheng, and K.Y. Tsang, *Supported mixed metal nanoparticles as electrocatalysts in low temperature fuel cells*, J. Mater. Chem. 14 (2004), pp. 505–516.
- [3] S. Eustis and M.A. El-Sayed, *Why gold nanoparticles are more precious than pretty gold: Noble metal surface plasmon resonance and its enhancement of the radiative and nonradiative properties of nanocrystals of different shapes*, Chem. Soc. Rev. 35 (2006), pp. 209–217.
- [4] K. Esumi, M. Wakabayashi, and K. Torigoe, *Preparation of colloidal silver-palladium alloys by UV-irradiation in mixtures of acetone and 2-propanol*, Col. Surf. A 109 (1996), pp. 55–62.
- [5] G.A. Gaddy, J.L. McLain, E.S. Steigerwalt, R. Broughton, B.L. Slaten, and G. Mills, *Photogeneration of silver particles in PVA fibers and films*, J. Clust. Sci. 12 (2001), pp. 457–471.
- [6] M. Harada and H. Einaga, *Photochemical deposition of platinum on TiO₂ by using poly(vinyl alcohol) as an electron donor and a protecting polymer*, Catal. Com. 5 (2004), pp. 63–67.
- [7] M. Harada and H. Einaga, *Formation mechanism of Pt particles by photoreduction of Pt ions in polymer solutions*, Langmuir 22 (2006), pp. 2371–2377.
- [8] A.S. Korchev, M.J. Bozack, B.L. Slaten, and G. Mills, *Polymer-initiated photogeneration of silver nanoparticles in SPEEK/PVA films: Direct metal photopatterning*, J. Am. Chem. Soc. 126 (2004), pp. 10–11.
- [9] M. Brust, J. Fink, D. Bethell, D.J. Schiffrin, and C. Kiely, *Synthesis and reactions of functionalised gold nanoparticles*, J. Chem. Soc., Chem. Com. (1995), pp. 1655–1656.
- [10] M. Brust, M. Walker, D. Bethell, D.J. Schiffrin, and R. Whyman, *Synthesis of thiol-derivatised gold nanoparticles in a two-phase liquid–liquid system*, J. Chem. Soc., Chem. Com. (1994), pp. 801–802.
- [11] C.-W. Chen, K. Arai, K. Yamamoto, T. Serizawa, and M. Akashi, *Temperature and pH dependence of the catalytic activity of colloidal platinum nanoparticles stabilized by poly[(vinylamine)-co-(N-vinylisobutyramide)]*, Macromol. Chem. Phys. 201 (2000), pp. 2811–2819.
- [12] X. Du, M. Inokuchi, and N. Toshima, *Preparation and characterization of Co-Pt bimetallic magnetic nanoparticles*, J. Magn. Magn. Mater. 299 (2006), pp. 21–28.
- [13] S. Eustis, *Gold and silver nanoparticles: Characterization of their interesting optical properties and the mechanism of their photochemical formation*, thesis, Georgia Institute of technology, Georgia, 2006.
- [14] M. Harada and H. Einaga, *Preparation of Pt/Rh bimetallic colloidal particles in polymer solutions using borohydride-reduction*, J. Coll. Int. Sci. 308 (2007), pp. 568–572.
- [15] P.V. Kamat, *Photophysical, photochemical and photocatalytic aspects of metal nanoparticles*, J. Phys. Chem. B 106 (2002), pp. 7729–7744.
- [16] J. Turkevich, P.C. Stevenson, and J. Hillier, *A study of the nucleation and growth processes in the synthesis of colloidal gold*, Discu. Faraday Soc. 11 (1951), pp. 55–75.
- [17] J.R. Morones, J.L. Elechiguerra, A. Camacho, K. Holt, J.B. Kouri, J.T. Ramirez, and M.J. Yacaman, *The bactericidal effect of silver nanoparticles*, Nanotechnology 16 (2005), pp. 2346–2353.
- [18] I. Sondi and B. Salopek-Sondi, *Silver nanoparticles as antimicrobial agent: A case study on E. coli as a model for Gram-negative bacteria*, J. Coll. Int. Sci. 275 (2004), pp. 177–182.
- [19] G.A. Martinez-Castan, N. Ninõ-Martinez, F. Martinez-Gutierrez, J.R. Martinez-Mendoza, and F. Ruiz, *Synthesis and antibacterial activity of silver nanoparticles with different sizes*, J. Nanopart. Res. 10 (2008), pp. 1343–1348.
- [20] T. Manerung, S. Tokura, and R. Rujiravanit, *Impregnation of silver nanoparticles into bacterial cellulose for antimicrobial wound dressing*, Carbohydr. Polym. 72 (2008), pp. 43–51.

- [21] S.T. Dubas, P. Kumlangdudsana, and P. Potiyaraj, *Layer-by-layer deposition of antimicrobial silver nanoparticles on textile fibers*, Col. Surf. A 289 (2006), pp. 105–109.
- [22] M. Anpo and M. Takeuchi, *The design and development of highly reactive titanium oxide photocatalysts operating under visible light irradiation*, J. Catal. 216 (2003), pp. 505–516.
- [23] O. Carp, C.L. Huisman, and A. Reller, *Photoinduced reactivity of titanium dioxide*, Prog. Solid State Chem. 32 (2004), pp. 33–177.
- [24] D. Hufschmidt, D. Bahnemann, J.J. Testa, C.A. Emilio, and M.I. Litter, *Enhancement of the photocatalytic activity of various TiO₂ materials by platinisation*, J. Photochem. Photobiol. A 148 (2002), pp. 223–231.
- [25] A.L. Linsebigler, G. Lu, and J.T. Yates, *Photocatalysis on TiO₂ surfaces: Principles, mechanisms, and selected results*, Chem. Rev. 95 (1995), pp. 735–758.
- [26] M. Ni, M.K.H. Leung, D.Y.C. Leung, and K. Sumathy, *A review and recent developments in photocatalytic water-splitting using TiO₂ for hydrogen production*, Ren. Sust. Ener. Rev. 11 (2007), pp. 401–425.
- [27] Y. Nosaka, K. Norimatsu, and H. Miyama, *The function of metals in metal-compounded semiconductor photocatalysts*, Chem. Phys. Lett. 106 (1984), pp. 128–131.
- [28] V. Subramanian, E. Wolf, and P.V. Kamat, *Semiconductor-metal composite nanostructures. To what extent do metal nanoparticles improve the photocatalytic activity of TiO₂ films?* J. Phys. Chem. B 105 (2001), pp. 11439–11446.
- [29] A.V. Vorontsov, E.N. Savinov, and J. Zhensheng, *Influence of the form of photodeposited platinum on titania upon its photocatalytic activity in CO and acetone oxidation*, J. Photochem. Photobiol. A 125 (1999), pp. 113–117.
- [30] J. Solla-Gullón, V. Montiel, A. Aldaz, and J. Clavilier, *Electrochemical characterisation of platinum nanoparticles prepared by microemulsion: How to clean them without loss of crystalline surface structure*, J. Electroanal. Chem. 491 (2000), pp. 69–77.
- [31] M. Gustavsson, H. Ekström, P. Hanarp, L. Eurenus, G. Lindbergh, E. Olsson, and B. Kasemo, *Thin film Pt/TiO₂ catalysts for the polymer electrolyte fuel cell*, J. Power Sources 163 (2007), pp. 671–678.
- [32] Y. Li, J. Petroski, and M.A. El-Sayed, *Activation energy of the reaction between Hexacyanoferrate(III) and thiosulfate ions catalyzed by platinum nanoparticles*, J. Phys. Chem. B 104 (2000), pp. 10956–10959.
- [33] F. Micoud, F. Maillard, A. Gourgaud, and M. Chatenet, *Unique CO-tolerance of Pt-WO_x materials*, Electrochem. Com. 11 (2009), pp. 651–654.
- [34] S. Von Kraemer, K. Wikander, G. Lindbergh, A. Lundblad, and A.E.C. Palmqvist, *Evaluation of TiO₂ as catalyst support in Pt-TiO₂/C composite cathodes for the proton exchange membrane fuel cell*, J. Power Sources 180 (2008), pp. 185–190.
- [35] H. Yang, N. Alonso-Vante, C. Lamy, and D.L. Akins, *High methanol tolerance of carbon-supported Pt-Cr alloy nanoparticle electrocatalysts for oxygen reduction*, J. Electrochem. Soc. 152 (2005), pp. A704–A709.
- [36] D. Riassetto, C. Holtzinger, M. Messaoud, S. Briche, G. Berthomé, F. Roussel, L. Rapenne, and M. Langlet, *Mechanisms involved in the platinization of sol-gel-derived TiO₂ thin films*, J. Photochem. Photobiol. A 202 (2009), pp. 214–220.
- [37] M. Langlet, A. Kim, M. Audier, C. Guillard, and J.M. Herrmann, *Liquid phase processing and thin film deposition of titania nanocrystallites for photocatalytic applications on thermally sensitive substrates*, J. Mater. Sci. 38 (2003), pp. 3945–3953.
- [38] M. Langlet, S. Permpoon, D. Riassetto, G. Berthome, E. Pernot, and J.C. Joud, *Photocatalytic activity and photo-induced superhydrophilicity of sol-gel derived TiO₂ films*, J. Photochem. Photobiol. A 181 (2006), pp. 203–214.
- [39] C. Millon, D. Riassetto, G. Berthomé, F. Roussel, and M. Langlet, *The photocatalytic activity of sol-gel derived photo-platinized TiO₂ films*, J. Photochem. Photobiol. A 189 (2007), pp. 334–348.

- [40] F. Maillard, E.R. Savinova, and U. Stimming, *CO monolayer oxidation on Pt nanoparticles: Further insights into the particle size effects*, J. Electroanal. Chem. 599 (2007), pp. 221–232.
- [41] R.E. Cameron and A.B. Bocarsly, *Multielectron-photoinduced reduction of chloroplatinum complexes: Visible light deposition of platinum metal*, Inorg. Chem. 25 (1986), pp. 2910–2913.
- [42] M. Avrami, *Kinetics of phase change. I general theory*, J. Chem. Phys. 7 (1939), pp. 1103–1112.
- [43] M. Avrami, *Kinetics of phase change. II transformation-time relations for random distribution of nuclei*, J. Chem. Phys. 8 (1940), pp. 212–224.
- [44] M. Avrami, *Kinetics of phase change. III granulation, phase change, and microstructure*, J. Chem. Phys. 9 (1941), pp. 177–184.
- [45] M.A. El-Sayed, *Some interesting properties of metals confined in time and nanometer space of different shapes*, Acc. Chem. Res. 34 (2001), pp. 257–264.
- [46] K.S. Ghosh, S. Kundu, M. Mandal, S. Nath, and T. Pal, *Studies on the evolution of silver nanoparticles in micelle by UV-photoactivation*, J. Nanopart. Res. 5 (2003), pp. 577–587.
- [47] R. Jin, Y. Cao, C.A. Mirkin, K.L. Kelly, G.C. Schatz, and J.G. Zheng, *Photoinduced conversion of silver nanospheres to nanoprisms*, Science 294 (2001), pp. 1901–1903.
- [48] P.V. Kamat, *Photoinduced transformations in semiconductormetal nanocomposite assemblies*, Pur. Appl. Chem. 74 (2002), pp. 1693–1706.
- [49] P.V. Kamat, M. Flumiani, and G.V. Hartland, *Picosecond dynamics of silver nanoclusters. Photoejection of electrons and fragmentation*, J. Phys. Chem. B 102 (1998), pp. 3123–3128.
- [50] D. Riassetto, C. Holtzinger, and M. Langlet, *Influence of platinum nano-particles on the photocatalytic activity of sol-gel derived TiO₂ films*, J. Mater. Sci. 44 (2009), pp. 2637–2646.
- [51] G. Chang, M. Oyama, and K. Hirao, *In situ chemical reductive growth of platinum nanoparticles on indium tin oxide surfaces and their electrochemical applications*, J. Phys. Chem. B 110 (2006), pp. 1860–1865.
- [52] F. Micoud, *Influence d'un support MO_x (M = W, Ti) Sur les propriétés électrocatalytiques de nanoparticules de platine*, thesis, Grenoble Institute of Technology, Grenoble, 2009.
- [53] T. Hanrath and B.A. Korgel, *Supercritical fluid-liquid-solid (SFLS) synthesis of Si and Ge nanowires seeded by colloidal metal nanocrystals*, Adv. Mater. 15 (2003), pp. 437–440.
- [54] W.L. Barnes, A. Dereux, and T.W. Ebbesen, *Surface plasmon subwavelength optics*, Nature 424 (2003), pp. 824–830.
- [55] K.R. Catchpole, S. Pillai, and K.L. Lin, *Novel Applications for Surface Plasmons in Photovoltaics*, Proceedings of 3rd World Conference on Photovoltaic Energy Conversion, Osaka, Japan, 2003, pp. 2714–2717.
- [56] W.R. Mason and H.B. Gray, *Electronic structures and spectra of square-planar gold(III) complexes*, Inorg. Chem. 7 (1968), pp. 55–58.
- [57] M.L. Marin, K.L. McGilvray, and J.C. Scaiano, *Photochemical strategies for the synthesis of gold nanoparticles from Au(III) and Au(I) using photoinduced free radical generation*, J. Am. Chem. Soc. 130 (2008), pp. 16572–16584.
- [58] S. Sato, K. Toda, and S. Oniki, *Kinetic study on the formation of colloidal gold in the presence of acetylenic glycol nonionic surfactant*, J. Coll. Int. Sci. 218 (1999), pp. 504–510.
- [59] J. Kimling, M. Maier, B. Okenve, V. Kotaidis, H. Ballot, and A. Plech, *Turkevich method for gold nanoparticle synthesis revisited*, J. Phys. Chem. B 110 (2006), pp. 15700–15707.
- [60] N.E. Christensen and B.O. Seraphin, *Relativistic band calculation and the optical properties of gold*, Sol. State Commun. 8 (1970), pp. 1221–1226.
- [61] N.E. Christensen and B.O. Seraphin, *Relativistic band calculation and the optical properties of gold*, Phys. Rev. B 4 (1971), pp. 3321–3344.
- [62] T.N. Angelidis, M. Koutlemani, and I. Poullos, *Kinetic study of the photocatalytic recovery of Pt from aqueous solution by TiO₂, in a closed-loop reactor*, Appl. Catal. B 16 (1998), pp. 347–357.
- [63] M. Epifani, C. Giannini, L. Tapfer, and L. Vasanelli, *Sol-Gel synthesis and characterization of Ag and Au nanoparticles in SiO₂, TiO₂, and ZrO₂ thin films*, J. Am. Cer. Soc. 83 (2000), pp. 2385–2393.

- [64] J. He, I. Ichinose, T. Kunitake, and A. Nakao, *In situ synthesis of noble metal nanoparticles in ultrathin TiO₂-gel films by a combination of ion-exchange and reduction processes*, Langmuir 18 (2002), pp. 10005–10010.
- [65] J. He, I. Ichinose, T. Kunitake, A. Nakao, Y. Shiraishi, and N. Toshima, *Facile fabrication of Ag-Pd bimetallic nanoparticles in ultrathin TiO₂-gel films: Nanoparticle morphology and catalytic activity*, J. Am. Chem. Soc. 125 (2003), pp. 11034–11040.
- [66] X. He, X. Zhao, and B. Liu, *Studies on a possible growth mechanism of silver nanoparticles loaded on TiO₂ thin films by photoinduced deposition method*, J. Non-Cryst. Solids 354 (2008), pp. 1267–1271.
- [67] E. Stathatos, P. Lianos, P. Falaras, and A. Siokou, *Photocatalytically deposited silver nanoparticles on mesoporous TiO₂ films*, Langmuir 16 (2000), pp. 2398–2400.
- [68] J.F. Pierson and C. Rousselot, *Stability of reactively sputtered silver oxide films*, Surf. Coat. Technol, 200 (2005), pp. 276–279.
- [69] M.C. Chen, S.D. Tsai, M.R. Chen, S.Y. Ou, W.H. Li, and K.C. Lee, *Effect of silver-nanoparticle aggregation on surface-enhanced Raman scattering from benzoic acid*, Phys. Rev. B 51 (1995), pp. 4507–4515.
- [70] S. Nie and S.R. Emory, *Probing single molecules and single nanoparticles by surface-enhanced Raman Scattering*, Science 275 (1997), pp. 1102–1106.